Optical Engineering

SPIEDigitalLibrary.org/oe

# Strategies for shortening the output pulse of silicon photomultipliers

José Manuel Yebras
Pedro Antoranz
José Miguel Miranda

# Strategies for shortening the output pulse of silicon photomultipliers

**José Manuel Yebras**
**Pedro Antoranz**
**José Miguel Miranda**
Universidad Complutense de Madrid
Dpto. Física Aplicada III, Facultad CC Físicas
Av. Complutense s/n, 28040, Madrid, Spain
E-mail: jmyebras@fis.ucm.es

**Abstract.** In this work, three strategies for shortening the output pulse of a silicon photomultiplier (SiPM) are reported. The first strategy is passive filtering, where band-pass filtering removes the lowest frequency components in the signal, getting a noticeable reduction in pulse width (a compression ratio of 10:1 was obtained). In the second place, a reflectometric scheme is proposed where the amplified signal coming from the SiPM is injected into a signal splitter with one of its stubs connected to a short-circuited stub. In the last strategy, the reflectometric part is replaced by an analog subtractor circuit. In this approach, a signal splitter with stubs of different lengths is used. All solutions provide good compression ratios, up to 10:1. Best pulses obtained are single narrow peaks, with width below 10 ns, preserving the photonic modulation and with good pseudo-Gaussian shape, single polarity and low ringing. The potential of pulse shortening for improving the capability of the detector to resolve single photons is demonstrated by mean of single photon counting patterns. The detection error probability is reduced in one order of magnitude when shortening is used for conditioning the output photosignal.  [DOI: 10.1117/1.OE.51.7.074004]

Subject terms: Geiger-mode avalanche photo-diodes; silicon photomultiplier; pulse shortening; single photon counting; reflectometry; active quenching.

Paper 111651 received Dec. 30, 2011; revised manuscript received May 30, 2012; accepted for publication May 31, 2012; published online Jul. 6, 2012.

## 1 Introduction

Silicon photomultipliers (SiPM), also known as Geiger-mode avalanche photo-diodes (GAPDs), are a new generation of photodetectors that provide very high sensitivity and show several advantages compared with more traditional devices (e.g., photomultipliers).[1,2] SiPMs present high gain and speed, low consumption level and polarization voltage, small size, immunity against magnetic fields, and an important potential for low cost production following standard MOS processes.[3–6] All of these facts allow one to postulate SiPMs as very interesting devices for photon detection applications in which high frequency and very low light intensity are involved.[7–10]

The SiPM is a matrix device where each cell is an avalanche photodetector (APD) working in Geiger mode that includes a quenching resistor.[3,4,11] This resistor is in charge of collapsing the avalanche process in each single APD, a short time after it starts. As all the cells in the device are connected to a common metallic grid, the total photocurrent is proportional to the number of fired cells. The typical response of the SiPM to an incoming light pulse is a very fast rising edge (avalanche is happening) followed by a slow downfall (avalanche has been quenched).[4,6]

The amplitude in the SiPM response signal is proportional to the number of impinging photons[4]. In other words, the amplitude of the current signal provided by the photodetector is amplitude modulated by the intensity of the optical exciting signal. This fact, together with the high sensitivity of the device (an avalanche process can be started even with only one incoming photon), allows the counting of number of photons reaching the photodetector. A large enough number of events will enable discrimination between $n$ and $n \pm 1$ photons, that is, for tracing the single photon counting (SPC) pattern of the system.[12–16] This can be done by tracing the pulse height spectrum taking into account the voltage or current signal provided by the SiPM. Also, those signals can be integrated and a spectrum expressed as the charge released by the detector as a function of the number of detected photons can be obtained. Both types of spectra are useful tools for comparing the performance of different detectors and for evaluating the benefit of photosignal processing techniques. In this work, pulse height spectra are used for demonstrating that photopulse shortening subsystems improve the SiPM capability for resolving photons.

Even for short light pulses ($\leq$10 ns), and depending on the features of the detector, the SiPM pulse width ranges from tens to hundreds of nanoseconds. This is a consequence of the long time constant provided by the micro-cell capacitance together with its high value quenching resistor. Those long photopulses are inconvenient because they lead to accumulation and reduction of the maximum allowable optical repetition frequency. The long tail in the photosignal happens when the detector is in the recovery time, which is not strictly a dead time. During that period, the SiPM is able to respond to new detections but with lower sensitivity. To solve this problem with no loss in sensitivity requires the use of active quenching techniques which, on the other hand, have to fight against parasitic signals that contaminate the photosignal of interest.[17–19] In a passive quenching scheme for low optical repetition frequencies, shortening of photopulses is advantageous. Because the informative content of the photosignal is

0091-3286/2012/$25.00 © 2012 SPIE

in the amplitude, the long tail in the pulse is unnecessary. Moreover, it is convenient to eliminate it for getting concentrated pulses that lead to good time-separation between consecutive pulses. Also, concentrated pulses are preferable for subsequent processing operations. For example, if an active quenching subsystem is planned for reducing the photodetector dead time, it is advisable to trigger it with short pulses. The major advantage of shortening strategies discussed in this work is not the pulse concentration itself. Shortening is providing a sort of signal filtering that result in a better separation between photosignal amplitudes corresponding to different number of impinging photons. As a consequence, the pulse height spectrum and the capability of the photodetector for resolving photons clearly improve. Comparison of SPC spectra with and without shortening shown later corroborates these facts and allows using several figures of merit for measuring the improvement provided by shortening.

## 2 Setup Design

Three different strategies for shortening the SiPM output pulse have been explored. All options have several common elements, being the bias circuit for the SiPM, the first one of them. The bias circuit for the SiPM used in the experiments (S10362-33-100 C[20,21]) is designed according to its manufacturer recommendation and can be seen in Fig. 1. $R_L$ is a limiting resistor for guarding the device, $R_S$ is the photocurrent sensing resistor, and $C_O$ is a blocking capacitor, whose aim is to remove any DC component in the signal. The biasing voltage is provided by the high accuracy power source Keithley model 6487.[22] The excitation pulse is obtained feeding the ultraviolet LED model HUVL400-5x0B (Hero Electronics) with the function generator Tektronix AFG3252 (2 GS/s, 240 MHz). The selected UV LED has the following specifications: central emission wavelength at 400 nm, close to the maximum photo-detection efficiency (PDE) of the SiPM (located at about 450 nm), spectral bandwidth of 20 nm and output power up to 2.2 mW with a half intensity angle of ±20-deg.[23] One end point of an optical fiber is properly connected to the LED and the other end point is connected to the SiPM. Both connections are properly made through plastic hoods that assure the mechanical fit and that provide luminous isolation. A deeper luminous isolation of the SiPM (for reducing as much as possible background events) is achieved covering the whole SiPM bias board with several layers of black cloths.

The amplitude of the output pulse is in the order of millivolts, so at least one gain stage must be added. For this purpose, the SiGe broadband MMIC amplifier BGA616 (Infineon Technologies[24]) has been selected. An optimized bias network (Fig. 2)[25] is required due to the DC bias and the RF output in this device share pin. Two aspects are critical on this network:

1. Inductors are used for providing a low impedance way for the biasing DC voltage and, at the same time, high impedance path for the outgoing high frequency signal.
2. Capacitors $C_1$–$C_3$ provide a simple and efficient way of removing spurious components coming from the DC voltage. This is done by distributing suppressing resonances in a wide bandwidth. Experimental determinations provide a mean gain value of 16 dB, a dynamic range of 1.5 V and a noise figure of 3.8 dB.

For getting signals with enough amplitude after shortening, it is necessary to provide higher gain, and this must be done by adding additional gain stages. The gain chain is completed adding two commercial pulse amplifiers (Fig. 3). These are ZPUL-21 (inverting[26]) and ZPUL-30P (non-inverting[27]), both from Mini-Circuits. ZPUL-21 has a mean gain factor of 10 dB (for experimental measurements ranging from 10 kHz to 700 MHz). ZPUL-30P shows a flatter gain factor around 31 dB for the range 10 kHz to 700 MHz. Attenuators have been inserted between elements

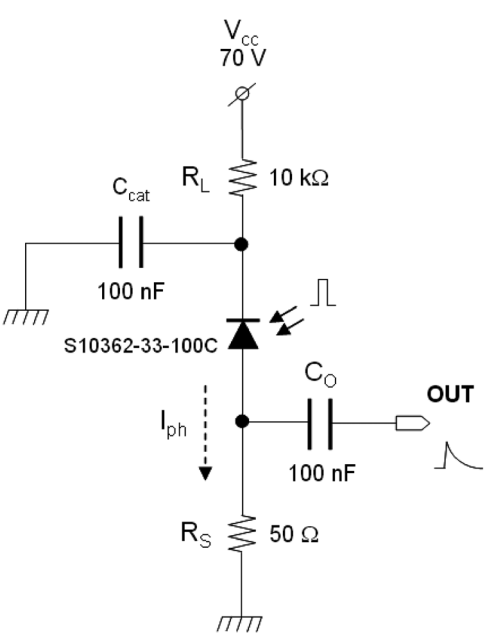


**Fig. 1** SiPM bias circuit.

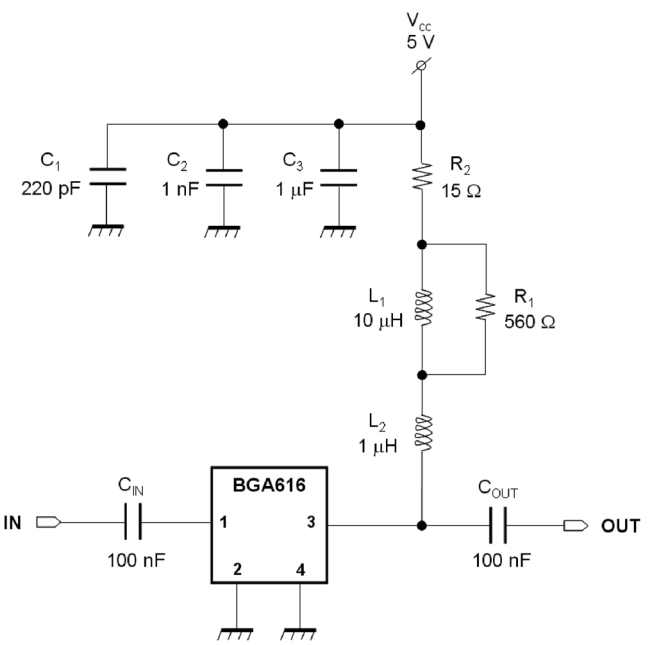


**Fig. 2** BGA616 MMIC amplifier bias network.

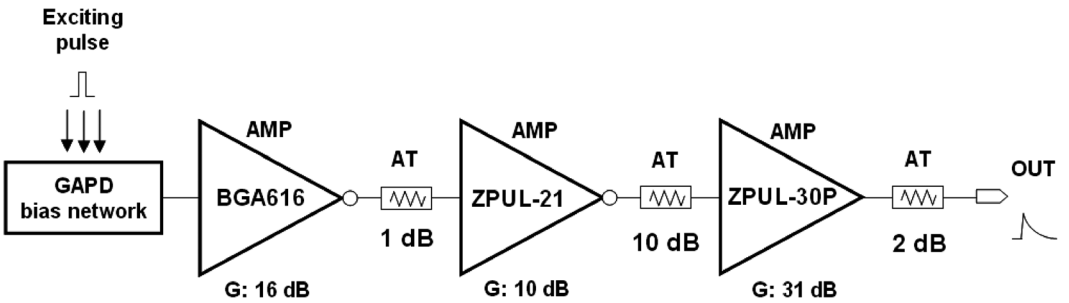


**Fig. 3** Gain chain used in the experiments. The GAPD bias network is an integrated board which includes both the photodetector and its bias network.

in the system with a triple purpose: impedance matching, ringing reduction, and dynamic range optimization (as a combination of the fixed values of the gain and attenuators value selection). The final stage of the chain could be a Schottky diode for removing negative signals and for reducing the ringing. Several different models of Schottky diodes have been tested, obtaining the best results with the model BAT17.[28]

The first shortening option consists on using a band-pass filter which removes the lowest frequency components of the signal, which are responsible for the slow falling edge. This filter will be included at the end of the processing chain. The second option proposes a reflectometric scheme, which can be seen in Fig. 4(a). The amplified signal coming from the SiPM is injected into a signal splitter and one of its stubs is connected to a short-circuited stub. The stub provides an inverted and delayed version of the original signal, so that the combination of both signals will be present in the free stub of the splitter. This signal should be fairly shorter than the original, but the fact that new peaks and ringing could appear must be taken into account.

The third solution is similar to the previous one, but by replacing the short-circuited stub by an analog subtractor circuit as shown in Fig. 4(b). The idea is to divide the signal coming from the photodetector and to apply a delay to one of the resulting signals. This way, one of the incoming signals to the subtractor is a delayed version (with no other modifications) of the other one. Two methods have been tested for obtaining the required delay:

1. A splitter with stubs of different lengths.
2. A splitter with stubs of equal lengths and a delayer device (opamp in buffer mode) in one of the stubs.

Best results have been obtained with the first option; so from now, it will be the only one taken into account. The operational amplifier LM7171 was selected for the subtractor circuit (the complete scheme is shown in Fig. 5) due to its very high speed operation (slew rate ~4100 V/μs).[29] Capacitor $C_1$ cancels the pole formed by the combination of the opamp input capacitance and the gain level setting resistors. Not cancelling this pole could cause instabilities in the circuit. Other possible causes for oscillation are the capacitive charges. For solving the problem, an isolating resistor, $R_{ISO}$, can be added at the output. That resistor, joint with the capacitive charge, makes a new pole that tends to stabilize the system. Capacitors in biasing lines have the same filtering purpose previously mentioned

## 3 Experimental Results

The result of adding a passive band-pass filter (whose 3 dB cutoff frequencies were 60 and 230 MHz) at the end of the processing chain is shown in Fig. 6, where it can be compared with the corresponding signal obtained without filtering. As it can be seen, the filter provides a noticeable reduction in pulse width (a compression relation of 10:1) respecting its sharp rising edge. But, at the same time, a reduction higher than 90% in the amplitude of the pulse happens. Despite this inconvenience, it is an interesting result

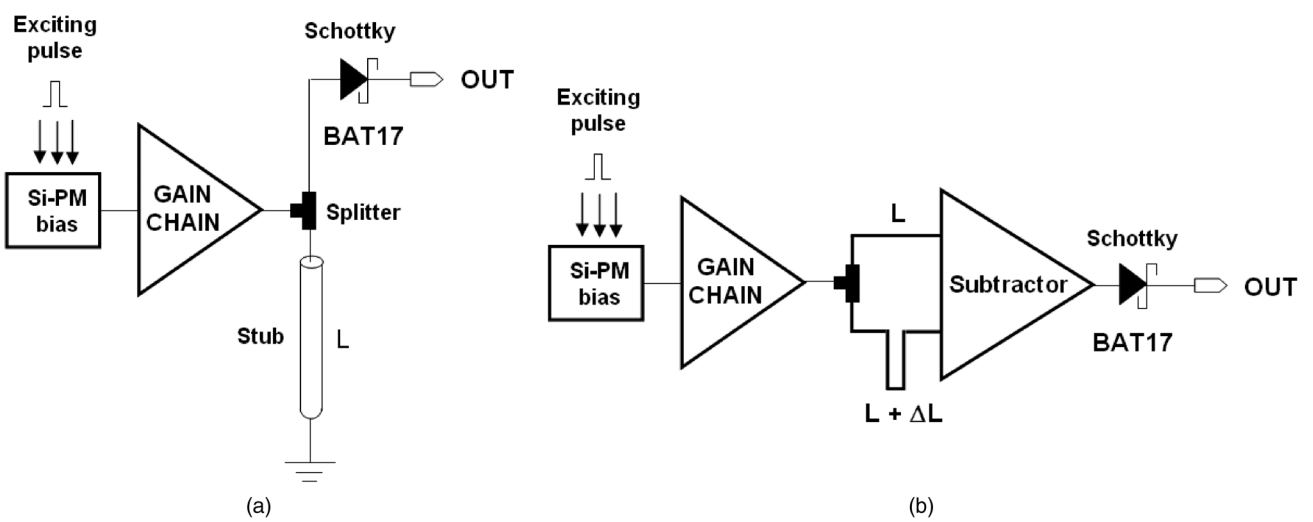


**Fig. 4** Pulse shortening system based on reflectometry (a) and on subtractor fed with stubs of different lengths (b).

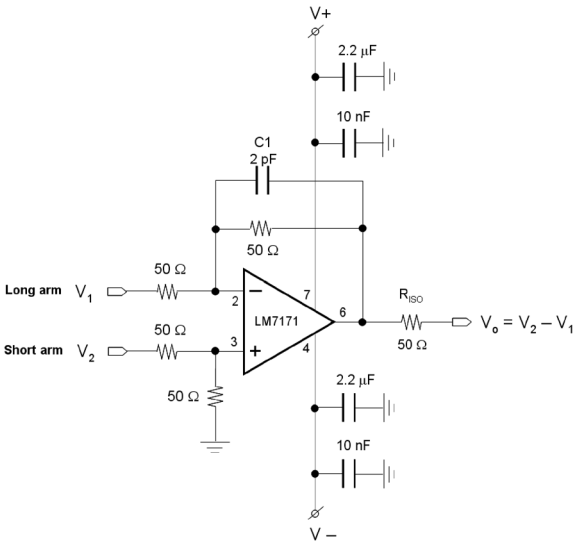


**Fig. 5** Complete subtractor circuit scheme.

because it demonstrates that a simple passive filtering is able to provide a substantial improvement in pulse conformation (pulses as short as 3 ns can be achieved). For avoiding such weak final amplitudes, higher gain or enhanced filtering could be provided. However, more sophisticated and flexible shortening schemes were used in order to overcome the limitations of this first approach.

Figure 7(a) illustrates the significant pulse compression and good shaping provided by the reflectometric shortening system [scheme in Fig. 4(a)] when comparing with the pulse obtained without shortening (scheme in Fig. 3). Also in this figure, the positive effect of inserting an appropriate Schottky diode as final element in the processing chain can be observed: the pulse is slightly shorter and undesirable slow negative parts in the signal are removed. Good compression ratio, nearly 3:1, was obtained, and in spite of a reduction of 40% in the amplitude, it is good enough for pulse manipulation. Figure 7(b) shows results obtained with the shortening system based on subtractor fed with stubs of different lengths. In this case, a compression

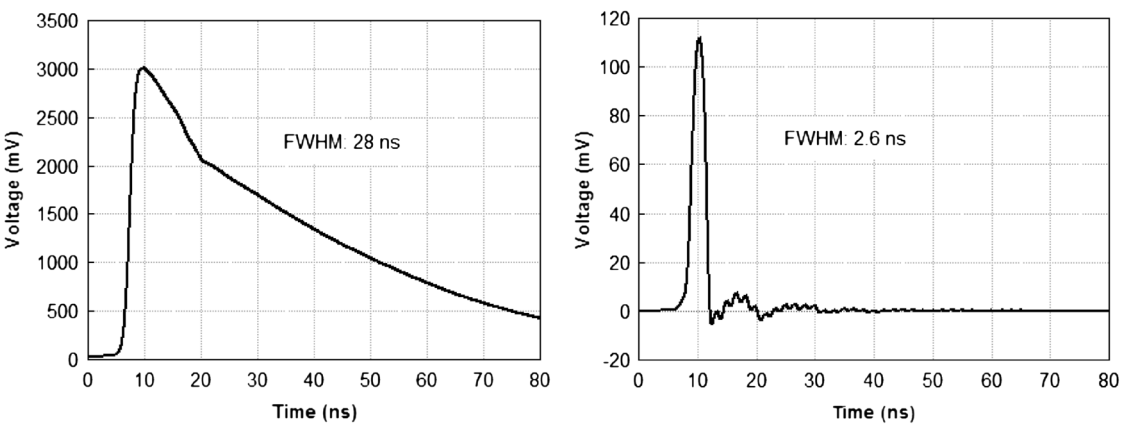


**Fig. 6** Pulse shortening adding a band-pass filter at the end of the processing chain. Incoming excitation pulses have FWHM of 10 ns. (a) Pulse without filtering, (b) pulse with band-pass filtering.

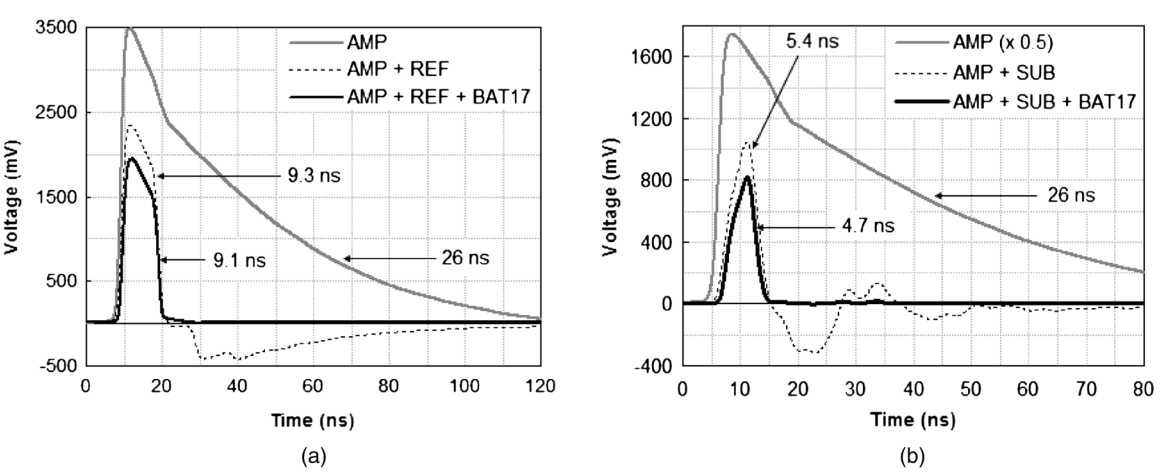


**Fig. 7** Comparing original output pulse with output using the reflectometric shortening scheme (a) and with the shortening system based on the subtractor with stubs of different lengths (b). In the rightmost figure, the original signal has been multiplied by 1/2 for better comparison with the other traces. For both cases, the input pulse FWHM is 10 ns. Length of the coaxial short-circuited stub (a): 102 cm. Difference in length between incoming stubs to subtractor (b): 102 cm.

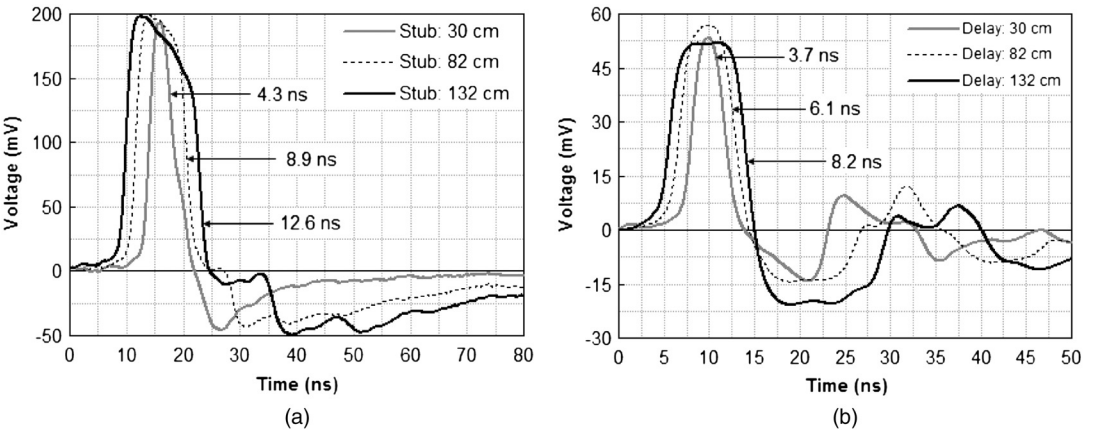


**Fig. 8** Width of shortened output pulse as a function of short-circuited stub length [for shortening system based on reflectometry, (a)] and of difference of length between input stubs [for shortening system based on subtractor, (b)]. Input pulse width of 10 ns were used.

ratio, nearly 6:1, is obtained, but with an undesirable loss of amplitude of around 80%.

A reduction of the stub length (or the difference in length between the input stubs to the subtractor) produces a reduction of the pulse full width at half maximum (FWHM). However, an excessive width reduction distorts the amplitude of the detected pulses, consequently affecting the SPC and reducing the capability of the photodetector for resolving photons. After several SPC experiments with these shortening systems, a good tradeoff was found when using coaxial stub lengths between 50 and 100 cm. Figure 8 shows typical pulse shapes for different stub lengths.

Figure 9 shows the output pulse amplitude as a function of the voltage of the electric pulses used for feeding the LED source. Figure 9(a) depicts the response of the SiPM (with no amplification stage) for two different biasing voltages. When the photonic density is high, there is higher probability that several photons fall simultaneously on the same pixel. This leads to a saturation effect that is clearly visible in Fig. 9(a). The extra electronic circuitry in the subtractor based shortening scheme reduces the linear dynamic range of the system. This can be verified by comparing Fig. 9(b) and 9(c), which show the response of the overall system with extra amplification and different shortening stages. The fact that the Schottky diode is not destroying the linearity of the system can also be observed in these figures.

The high frequency digital oscilloscope, Agilent Infiniium DSO81204B (12 GHz, 40 GSa/s), allows tracing and saving amplitude histograms.[30] Its histogram utility works like a multichannel analyzer. Figure 10 shows the pulse height spectra obtained when no shortening and the reflectometric shortening scheme are used. The improvement provided by the shortening subsystem is evident. More photopeaks are distinguishable and they are narrower and more intense. This last fact is a demonstration of that shortening, as it was previously mentioned, that is being able to reduce the amplitude dispersion on pulses corresponding to the same number of detected photons. The consequence of this, as it is clearly shown in Fig. 10, is the ability to resolve the peaks that significantly improves when shortening is used.

Several figures of merit can be used for comparing both spectra and for characterizing the photodetector capability to resolve photons in both cases. The weak photon emission and detection must reveal a Poisson distribution.[31] So, the first figure of merit might be the degree of fitting of the experimental histogram by mean of a distribution resulting from the convolution of a Gaussian function (simulating the

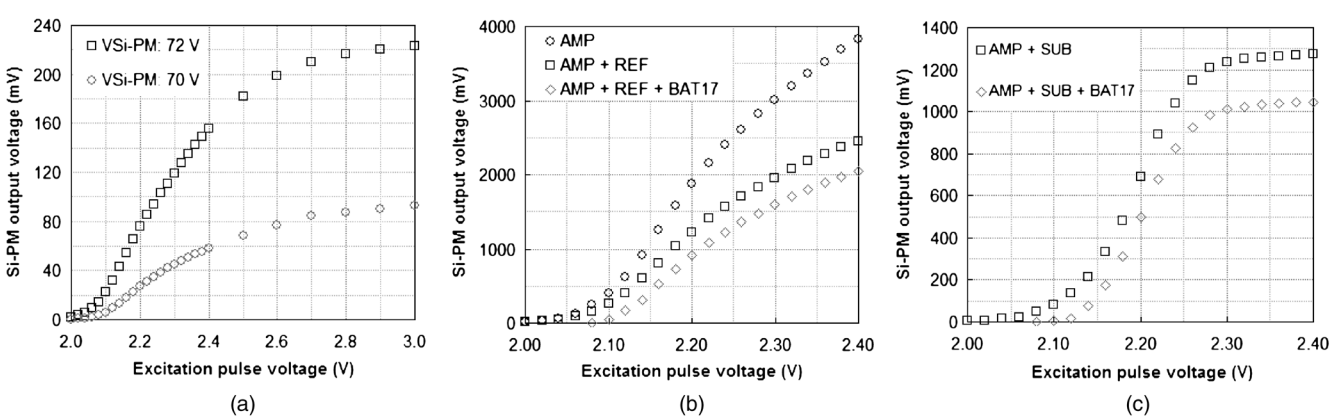


**Fig. 9** System response as a function of the input LED pulse amplitude. (a) Only SiPM was used, for two different biasing voltages (70 V, 72 V). (b) SiPM and amplification (circles); SiPM, amplification and reflectometry-based shortener (squares); SiPM, amplification and shortener with Schottky diode (diamonds). (c) SiPM, amplification and subtractor-based shortener (squares); SiPM, amplification and shortener with Schottky diode (diamonds). In all measurements shown in (b) and (c) the SiPM biasing voltage was 70 V.

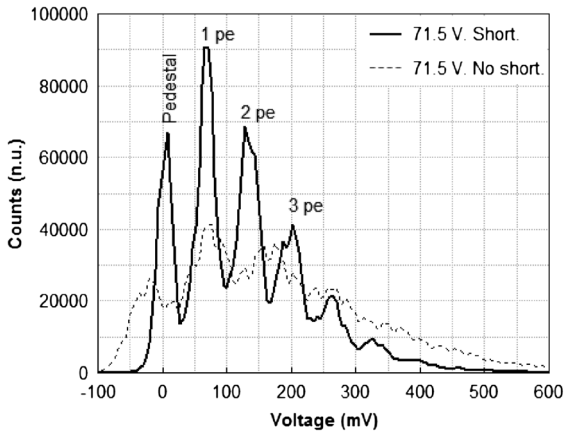


**Fig. 10** Pulse height spectra obtained when no shortening is used (dashed line) and when reflectometric shortening scheme is used (solid line). The SiPM biasing voltage in both cases was 71.5 V.

non-ideal peak in the spectrum) with a Poisson distribution. For implementing the simulation, it was taken into account that the mean value of the $n$th peak in the spectrum must be $n$ times the mean value for the 1 photoelectron peak and that the typical deviation of the $n$th peak is approximately the typical deviation corresponding to the 1 photoelectron peak multiplied by the square root of $n$.[32] The fit of the spectrum obtained when shortening is used can be seen in Fig. 11. In this figure, the experimental histogram has been replaced by its corresponding probability density function. Simulation it says that the mean voltage corresponding to the single photoelectron is 65 mV, with a typical deviation of 13 mV, and that a number of 2.2 photoelectrons are being detected on average (this value corresponds to the parameter of the final Poisson distribution that best fits the experimental data). Despite of the underestimation of the pedestal peak, quite accurate fit is possible when shortening is used. However, the fit of the spectrum when no shortening is used does not provide an acceptable result, since neither the peaks are correctly located nor their heights can properly be adjusted.

The figure of merit named as peak-valley-peak relation (PVPR) provides a measurement of the proportion in

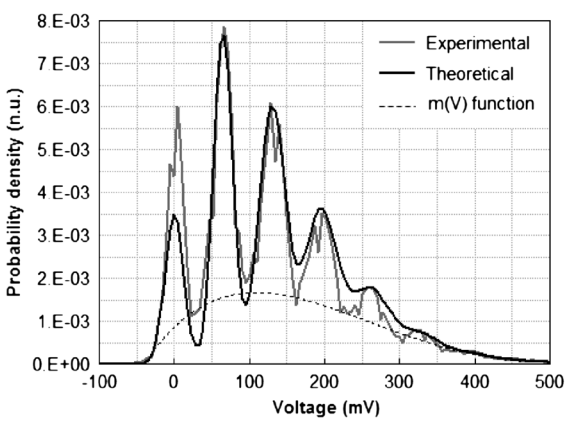


**Fig. 11** Fit of the probability density function obtained when shortening is used (gray line) by mean of the convolution of a Gaussian function with a Poisson distribution (black line). The function that fits the baseline elevation created by the overlapping of the peaks in the spectrum is also shown (dashed line).

which a certain peak is above the baseline elevation caused by the overlapping of the different peaks. It is a dimensionless quantity whose ideal value is 1. The valley value for a certain peak is the highest one flanking its maximum.

$$\text{PVPR} = \frac{\text{Peak maximum} - \text{Peak valley}}{\text{Peak maximum}} \ [n.u.];$$
$$\text{Ideal: PVPR} = 1; \ \text{Real: } 0 < PVPR < 1. \tag{1}$$

The so called quality parameter (QP) is a measurement of the width of the peaks in the spectrum. The FWHM of the peak is referred to the voltage corresponding to the single photoelectron. Thus, QP expresses the width of the peaks in terms of number of photoelectrons and its ideal value is 0. As QP grows toward 1, the overlapping of peaks in the spectrum is quite notable.

$$\text{QP} = \frac{\text{Peak deviation}}{\text{Voltage for 1 pe}} \ [\text{pe}];$$
$$\text{Ideal: QP} = 0; \quad \text{Real: QP} > 0. \tag{2}$$

It is possible to fit the baseline elevation created by the overlapping of the peaks in the spectrum by mean of a polynomial function $m(V)$. This function $m(V)$, where $V$ is the photosignal voltage, is accurate enough for all the voltages of interest, between a low voltage $L$ and a high voltage $H$ (both empirically determined). The so called form factor (FF) of the spectrum is defined as the ratio between the integral of the spectrum above the baseline elevation referred to the whole integral of the spectrum. It is a measurement that quantifies the relevance of that overlapping on limiting the photon resolution of the system. Being $h(V)$ the function that expresses the probability density function corresponding to the experimental histogram, the form factor, whose ideal value is 1, is defined as shown in the following equation:

$$\text{FF} = \frac{\int_L^H h(V) \cdot \mathrm{d}V - \int_L^H m(V) \cdot \mathrm{d}V}{\int_L^H h(V) \cdot \mathrm{d}V} \ [n.u.];$$
$$\text{Ideal: FF} = 1; \quad \text{Real: } 0 < \text{FF} < 1. \tag{3}$$

But perhaps the most informative figure of merit might be the detection error probability, defined as the probability of deciding the detection of $n \pm 1$ photons, when $n$ photons have really been detected. Figure 12(a) shows the fit of the experimental histogram when shortening is used by mean of Gaussian functions simulating each peak. Individual Gaussian functions are depicted as dashed lines, whereas their sum is shown as a solid line that fits quite well the experimental probability density. Figure 12(b) shows the portion of the Gaussian function corresponding to two photoelectrons that is providing detection error. Naming as $L_{\text{error}}$ and $H_{\text{error}}$ the points in which the Gaussian function for $n$ photoelectrons, $g_n(V)$, coincides with the Gaussian functions corresponding to $n-1$ and $n+1$ photoelectrons, $g_{n-1}(V)$ and $g_{n+1}(V)$ respectively, the detection error probability (DEP) for the $n$th peak is defined as shown in Eq. (4).

$$\text{DEP} = \frac{\int_{-\infty}^{L_{\text{error}}} g_n(V) \cdot \mathrm{d}V + \int_{H_{\text{error}}}^{\infty} g_n(V) \cdot \mathrm{d}V}{\int_{-\infty}^{\infty} g_n(V) \cdot \mathrm{d}V};$$
$$\text{Ideal: DEP} = 0; \quad \text{Real: DEP} > 0. \tag{4}$$

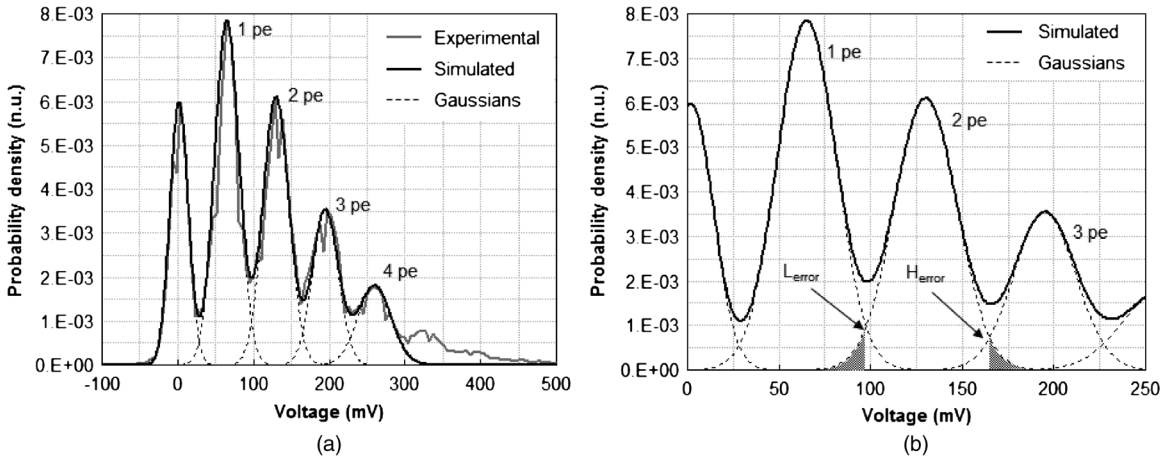


**Fig. 12** (a) Fit of the probability density function obtained when shortening is used (gray line) by mean of the sum (black solid line) of Gaussian functions (dashed line). (b) Areas causing detection error for the case of 2 photoelectrons.

**Table 1** Figures of merit when using the SiPM with and without reflectrometry based pulse shortening. Improvements when using shortening have been achieved in all cases.

| | No shortening | | | | Shortening | | | | Improvement when using shortening | | | |
|---|---|---|---|---|---|---|---|---|---|---|---|---|
| | PVPR (n.u) | QP (pe) | FF (n.u) | Error (%) | PVPR (n.u) | QP (pe) | FF (n.u) | Error (%) | $PVPR_{improv.}$ (%) | $QP_{improv.}$ (%) | $FF_{improv.}$ (%) | $Error_{improv.}$ (%) |
| ideal | 1 | 0 | 1 | 0 | 1 | 0 | 1 | 0 | | | | |
| 1 pe | 0.48 | 1.17 | 0.24 | 33.7 | 0.76 | 0.58 | 0.51 | 3.2 | 58 | 50 | 113 | 91 |
| 2 pe | 0.42 | 1.66 | | 52.8 | 0.69 | 0.66 | | 5.3 | 64 | 60 | | 90 |
| 3 pe | 0.26 | 1.66 | | 80.8 | 0.61 | 0.77 | | 7.3 | 135 | 54 | | 91 |

Table 1 summarizes all the previous figures of merit for both cases, when no shortening is used and when shortening based on reflectometry is used. Also, the improvement obtained thanks to the shortening subsystem referred to the case of no shortening is included in the table. All parameters demonstrate significant enhancement in the SPC pattern, when shortening is used. But perhaps, the most interesting and comprehensive result obtained is that the detection error probability has been reduced in one order of magnitude. The high error probability happening when using the SiPM alone (from 33% to 80%) has been reduced to less than 8% for any number of photoelectrons.

## 4 Conclusions

Three strategies for shortening the output pulse provided by a silicon photomultiplier have been discussed in this work. The first solution is based on applying a simple band-pass filtering to the amplified signal. It has been shown that a compression ratio of 10:1 can be obtained, but at the cost of an unacceptable loss in pulse amplitude. Two other options have been tested; reflectometry based shortening system and subtractor based shortening system. They provide good compression ratios up to 6:1. Best results in terms of pulse duration, ringing suppression, pulse shaping, dynamic range, and capability for tracing well defined SPC patterns were obtained with the reflectometric shortening system using a coaxial short-circuited stub in the order of 50 to 100 cm. In addition, the losses in the reflectometric system are 50% lower than in the subtractor system.

The most interesting result obtained when using pulse shortening is the dramatic improvement in photon resolution with SiPMs of large area, which provide poor counting results when working alone. Several figures of merit have been used for characterizing SPC patterns, and we have demonstrated that shortening achieves noticeable improvements in all of them. The proposed reflectometric technique considerably reduces the pulse width with a marginal reduction of the amplitude. This accomplishment is useful for signal processing and for feeding other subsystems that will act on the SiPM behavior (e.g., active quenching circuits). Patterns obtained by means of shortening, as opposed to those measured when the SiPM is used alone, are adjustable by means of simple Poissonian distributions, have clearly defined and separable photopeaks and provide a very important reduction in the DEP. When SiPM is used alone, DEP ranges from 30% to 80%, depending on the considered photopeak, but it is lower than 8% for any photopeak when the shortening subsystem is used.

## Acknowledgments

This work has been funded by spanish MICINN Project FPA2010-22056-C06-04.

## References

1. D. Renker, "Geiger-mode avalanche photodiodes, history, properties and problems," *Nucl. Instrum. Meth. A* **567**(1), 48–56 (2006).
2. V. Kovaltchouk et al., "Comparison of a silicon photomultiplier to a traditional vacuum photomultiplier," *Nucl. Instrum. Meth. A* **538**(1–3), 408–415 (2005).
3. D. Renker and E. Lorenz, "Advances in solid state photon detectors," *J. Instrum.* **4**(4), P04004 (2009).
4. J. Haba, "Status and perspectives of pixelated photon detector (PPD)," *Nucl. Instrum. Meth. A* **595**(1), 154–160 (2008).
5. D. Renker, "New trends on photodetectors," *Nucl. Instrum. Meth. A* **571**(1–2), 1–6 (2007).
6. A. Stewart et al., "Study of the properties of new SPM detectors," *Proc. SPIE* **6119**, 61190A (2006).
7. I. Johnson et al., "A Geiger-mode avalanche photodiode array for X-ray photon correlation spectroscopy," *J. Synchrotron Radiat.* **16**(1), 105–109 (2009).
8. S. Korpar et al., "Silicon photomultiplier as a detector of Cherenkov photons," *Nucl. Instrum. Meth. A* **595**(1), 161–164 (2008).
9. N. Otte et al., "The potential of SiPM as photon detector in astroparticle physics experiments like MAGIC and EUSO," *Nucl. Phys. B- Proc. Suppl.* **150**(1–3), 144–149 (2006).
10. J. Kataoka et al., "Recent progress of avalanche photodiodes in high-resolution X-rays and gamma-rays detection," *Nucl. Instrum. Meth. A* **541**(1–2), 398–404 (2005).
11. Z. Sadygov et al., "Three advanced designs of micro-pixel avalanche photodiodes: their present status, maximum possibilities and limitations," *Nucl. Instrum. Meth. A* **567**(1), 70–73 (2006).
12. J. O'Keeffe, C. Jackson, and H. Brüggemann, "New developments in photon counting modules," (2007), http://www.laser2000.de/fileadmin/Produktdaten/SEN/Photonik_01_2006_SENSL_engl.pdf, (13 June 2012).
13. C. Jackson and A. Mathewson, "Improvements in silicon photon counting modules," *Proc. SPIE* **5726**, 69–76 (2005).
14. Hamamatsu, "MPPC multi-pixel photon counter," (2009), http://sales.hamamatsu.com/assets/applications/SSD/mppc_kapd0002e08.pdf, (13 June 2012).
15. Hamamatsu, "Photon counting using photomultiplier tubes," (2001), http://sales.hamamatsu.com/assets/applications/ETD/PMT_photoncounting.pdf, (13 June 2012).
16. S. Bellis, R. Wilcock, and C. Jackson, "Photon counting imaging: the DigitalAPD," *Proc. SPIE* **6068**, 60680D (2006).
17. F. Zappa et al., "SPICE modeling of single photon avalanche diodes," *Sensor. Actuat. A-Phys.* **153**(2), 197–204 (2009).
18. A. Gallivanoni et al., "Monolithic active quenching and picosecond timing circuit suitable for large-area single-photon avalanche diodes," *Opt. Express* **14**(12), 5021–5030 (2006).
19. F. Zappa et al., "Monolithic active-quenching and active-reset circuit for single-photon avalanche detectors," *IEEE J. Solid-St. Circ.* **38**(7), 1298–1301 (2003).
20. Hamamatsu, "MPPC S10362-33 series-S10931 series," (2009), http://sales.hamamatsu.com/assets/pdf/parts_S/s10362-33series_kapd1023e05.pdf, (13 June 2012).
21. Hamamatsu, "Characteristics and use of SiAPD (avalanche photodiode)," (2001), http://sales.hamamatsu.com/assets/applications/SSD/Characteristics_and_use_of_SI_APD.pdf, (13 June 2012).
22. Keithley Instruments Inc. "6487 Picoammeter/Voltage source," (2009), http://www.keithley.com/data?asset=10756, (13 June 2012).
23. Hero Electronics. "HUVL400-5x0B high power ultraviolet LEDs," *data sheet* (2002), http://common.leocom.jp/datasheets/153506_9741.pdf.
24. Infineon Technologies. "BGA616 silicon germanium groadband MMIC amplifier," (2001), http://www.datasheetcatalog.org/datasheet/infineon/1-bga616_1.pdf, (13 June 2012).
25. P. Antoranz, "Contributions to the high frequency electronics of MAGIC II gamma ray telescope," PhD thesis, (Universidad Complutense Madrid 2009), http://eprints.ucm.es/10587/.
26. Mini-Circuits. "ZPUL-21 coaxial pulse amplifier-50 Ω inverting-0.0025 to 700 MHz," (2010), http://www.minicircuits.com/pdfs/ZPUL-21.pdf, (13 June 2012).
27. Mini-Circuits. "ZPUL-30P coaxial pulse amplifier-50 Ω non-inverting-0.0025 to 700 MHz," (2010), http://www.minicircuits.com/pdfs/ZPUL-30P.pdf, (13 June 2012).
28. NXP-Philips, "BAT17 Schottky barrier diode," (2003), http://www.nxp.com/documents/data_sheet/BAT17.pdf, (13 June 2012).
29. National Semiconductor, "LM7171 very high speed, high output current, voltage feedback amplifier," (2006), http://www.national.com/ds/LM/LM7171.pdf, (13 June 2012).
30. Agilent Technologies, "DSA80000B digital signal analyzer 2 GHz to 13 GHz oscilloscope measurement systems," (2006), http://cp.literature.agilent.com/litweb/pdf/5989-5811EN.pdf, (13 June 2012).
31. M. Ramilli et al., "Photon-number statistics with silicon photomultipliers," *J. Opt. Soc. Am. B* **27**(5), 852–862 (2010).
32. V. Saveliev, "Silicon photomultiplier: physics, development and applications," (2006), http://f64.nsstc.nasa.gov/colloquia/abstracts_spring06/presentations/VSaveliev.pdf, (13 June 2012).

**José Manuel Yebras** received his degree in electrical engineering (specialty in Electronics) from the Universidad Politécnica de Madrid in 1998; and in 2010, he graduated as master in biomedical physics from the Universidad Complutense de Madrid. From 1999 through 2004, he was working as $R + D$ engineer in the Laboratory of InfraRed sensors (LIR) in the Universidad Carlos III de Madrid. From 2010, he is working with high sensitivity photodetectors at the Microwaves Group, Department of Applied Physics III, Faculty of Physical Sciences, Universidad Complutense de Madrid. He has also worked for 5 years in multinational companies (Siemens Medical Solutions, Chep España, and Amper Sistemas) developing technological innovation projects. He is co-inventor of one patent in use by EADS Construcciones Aeronáuticas, which was extended to Europe and United States of America. His areas of interest in research are focused in Applied Physics, and especially in the field of Biomedical Physics.

**Pedro Antoranz** received the degree in physics at the Universidad Autónoma de Madrid (UAM) in 2000, and the degree in electronic engineering at the Universidad Complutense de Madrid (UCM) in 2003. He also received his PhD in physics at the Universidad Complutense in 2009. He is an expert in the design of integrated circuits and testing boards for signal integrity in electronic subsystems and also in the characterization of high sensitivity photodetectors. He has designed, produced and tested different prototypes for photodetection signal conditioning, as well as in ns-range pulse generators. His designs have been integrated into the electronics of particle physics experiments, and they are directly pertinent for fluorescence measuremet systems. In 2006 he received his nomination as "Professor Ayudante" in the Department of Applied Physics III of the UCM, and in 2011 he was promoted to "Ayudante Doctor", position that he currently holds.

**Jose Miguel Miranda** received his PhD degree in 1998. His doctoral thesis was awarded with the prize 'Premio Extraordinario de Doctorado' at the Faculty of Physics of the University Complutense of Madrid (UCM). In 2002 he was appointed permanent lecturer in the speciality of Electromagnetics, and in 2009 received a special mention for being among the 5% top rated educators at UCM. In 2011 he was awarded with the full professor accreditation by the Spanish national agency ANECA. He has been visiting researcher at the California Institute of Technology, the Institut für Hochfrequenztechnik of Darmstadt and the Chalmers University of Goteborg. He is one of the founders of the master in biomedical physics offered by UCM, and is the author of the book "Ingenieria de Microondas", published by Pearson Editorial. His present research interests include high frequency and low noise electronics, as well as ultrafast solid state photodetectors for Cherenkov Telescope installations (MAGIC and CTA).